Gating has a negligible impact on dose delivered in MRI-guided online adaptive radiotherapy of prostate cancer

Wahlstedt, Isak; Andratschke, Nicolaus; Behrens, Claus P.; Ehrbar, Stefanie; Gabryś, Hubert S.; Schüler, Helena Garcia; Guckenberger, Matthias; Smith, Abraham George; Tanadini-Lang, Stephanie; Tascón-Vidarte, José D.

Total number of authors:
12

Published in:
Radiotherapy and Oncology

Link to article, DOI:
10.1016/j.radonc.2022.03.013

Publication date:
2022

Document Version
Publisher's PDF, also known as Version of record

Radiotherapy and Oncology 170 (2022) 205–212

Contents lists available at ScienceDirect

Radiotherapy and Oncology

journal homepage: www.thegreenjournal.com

Original Article

Gating has a negligible impact on dose delivered in MRI-guided online adaptive radiotherapy of prostate cancer

Isak Wahlstedt [a,b,c,*], Nicolaus Andratschke [d], Claus P. Behrens [a,c], Stefanie Ehrbar [d], Hubert S. Gabryś [d], Helena Garcia Schüler [d], Matthias Guckenberger [d], Abraham George Smith [e], Stephanie Tanadini-Lang [d], José D. Tascón-Vidarte [e], Ivan R. Vogelius [b,f], Janita E. van Timmeren [d]

[a] Department of Health Technology, Technical University of Denmark, Kongens Lyngby; [b] Department of Oncology, Centre for Cancer and Organ Diseases, Copenhagen University Hospital - Rigshospitalet; [c] Department of Oncology, Copenhagen University Hospital - Herlev and Gentofte, Herlev, Denmark; [d] Department of Radiation Oncology, University Hospital Zurich, University of Zurich, Switzerland; [e] Department of Computer Science, University of Copenhagen; and [f] Department of Health and Medical Sciences, University of Copenhagen, Denmark

ARTICLE INFO

Article history:
Received 13 December 2021
Received in revised form 21 March 2022
Accepted 23 March 2022
Available online 26 March 2022

Keywords:
Radiotherapy
Margin assessment
Adaptive radiotherapy
MR-guided radiotherapy
Prostate cancer
Prostate motion
Motion-mitigation
Beam-gating
Dose accumulation
Deformable image registration

ABSTRACT

Background and purpose: MR-guided radiotherapy (MRgRT) allows real-time beam-gating to compensate for intra-fractional target position variations. This study investigates the dosimetric impact of beam-gating and the impact of PTV margin on prostate coverage for prostate cancer patients treated with online-adaptive MRgRT.

Materials and methods: 20 consecutive prostate cancer patients were treated with online-adaptive MRgRT SBRT with 36.25 Gy in 5 fractions (PTV $D_{95\%} \geq 95\%$ ($N = 5$) and PTV $D_{95\%} \geq 100\%$ ($N = 15$)). Sagittal 2D cine MRIs were used for gating on the prostate with a 3 mm expansion as the gating window. We computed motion-compensated dose distributions for (i) all prostate positions during treatment (simulating non-gated treatments) and (ii) for prostate positions within the gating window (gated treatments). To evaluate the impact of PTV margin on prostate coverage, we simulated coverage with smaller margins than clinically applied both for gated and non-gated treatments. Motion-compensated fraction doses were accumulated and dose metrics were compared.

Results: We found a negligible dosimetric impact of beam-gating on prostate coverage (median of 0.00 Gy for both $D_{95\%}$ and D_{mean}). For 18/20 patients, prostate coverage ($D_{95\%} \geq 100\%$) would have been ensured with a prostate-to-PTV margin of 3 mm, even without gating. The same was true for all but one fraction.

Conclusion: Beam-gating has negligible dosimetric impact in online-adaptive MRgRT of prostate cancer. Accounting for motion, the clinically used prostate-to-PTV margin could potentially be reduced from 5 mm to 3 mm for 18/20 patients.

The standard dose prescription for external beam radiotherapy (EBRT) of prostate cancer has been 74–78 Gy in 1.8–2.0 Gy per fraction. However, during the last decade, randomized trials of dose-escalated EBRT (doses $\geq$ 75.6 Gy) [1], hypofractionation [2–6], focal boosting of the macroscopical tumor [7,8], and multiple and single-fractionation prostate stereotactic body radiotherapy [9] have changed the clinical practice. The increasing use of these hypofractionated regimens implies unprecedented demands on the accuracy of treatment delivery. For extreme hypofractionation (7–8 Gy per fraction), the ESTRO ACROP consensus guideline on the use of image guided radiation recommends monitoring and ideally tracking [10]. To date, only a few systems, such as electromagnetic transponder-based systems and single/stereoscopic kilovoltage imaging of implanted markers [11,12] allow continuous intra-fractional target monitoring. Recently introduced magnetic resonance linear accelerators (MR-linacs) allow for continuous target monitoring [13]. Furthermore, the MRIdian MR-linac [14] utilizes automated image-guided beam-gating for compensation of intra-fractional target position uncertainties.

Electromagnetic transponder-based systems such as the Calypso system have been shown to improve the dosimetric accuracy of prostate stereotactic body radiotherapy (SBRT) in phantom studies, for gating [15], couch tracking [15–17], and multileaf collimator tracking [15,17]. De Roover et al. [15] applied three motion traces to two SBRT treatments, planned with focal boost according to the hypo-FLAME trial [8]. They showed that couch tracking, MLC tracking, and beam-gating with Calypso were all able to compensate for prostate rotation, improving dosimetric accuracy. Of the

* Corresponding author at: Rudolph Berghs Gade 37, Stuen, 2100 Copenhagen, Denmark.
E-mail address: isak.hannes.wahlstedt@regionh.dk (I. Wahlsted.

https://doi.org/10.1016/j.radonc.2022.03.013
0167-8140/

three, gating achieved the best organs at risk (OAR) sparing. Colvill et al. [18] employed an in-house dose reconstruction approach to evaluate the potential dosimetric impact of gating and MLC tracking for 20 fractions belonging to five prostate cancer patients receiving conventionally fractionated radiotherapy. They found that both gating and MLC tracking could improve target dose coverage for a small number of individual fractions. Kontaxis et al. [19] and Menten et al. [20] both reconstructed the dose for five prostate cancer patients treated on an Elekta Unity MR-linac. In both studies, the real-time MR images (MRIs) were not used for beam-interruption nor motion mitigation but for retrospective dose reconstruction only.

MR-guided beam-gated radiotherapy, as implemented in the MRIdian MR-linac [14], is offering marker-free non-invasive gating on the prostate. However, according to a recent review [21], there is no current research establishing the dosimetric impact of beam-gating for MR-guided radiotherapy (MRgRT) for hypofractionated prostate cancer. In this retrospective study on 20 patients with prostate cancer, we investigate the dosimetric impact of beam-gating in online-adaptive MRgRT SBRT. Furthermore, we explore whether the clinically used prostate-to-PTV margin could have been reduced while still retaining the prescription dose to the prostate, implying tangible benefits for the patients in terms of reduced dose to healthy tissue.

Materials and methods

Patients

This study includes all prostate cancer patients (N = 20), treated from the commissioning of the MR-linac in April 2019 until June 2021. The inclusion criteria were SBRT with 5 fractions of 7.25 Gy, treated with online-adaptive MRgRT in all fractions with automated beam-gating based on sagittal cine MRIs acquired at 4 frames per second (FPS) and a gating window that was defined as a 3 mm margin from the prostate (Fig. 1). All patients were treated with step-and-shoot intensity-modulated radiotherapy. The prostate-to-PTV-margin was 3 mm posteriorly and 5 mm in all other directions. For 15 patients the coverage criterion was that 95% of the PTV should receive at least 36.25 Gy ($D_{95\%} \geq 100\%$) whereas for the first 5 patients it was $D_{95\%} \geq 95\%$. All other planning objectives and dose constraints are provided in Table S1 in Supplementary file 1. Patients were treated with daily plan adaptation, including daily correction of the prostate structure, on a MRIdian MR-linac (ViewRay Inc., Mountain View, CA) [14] and immobilized using a knee and ankle fixation. On a sagittal slice of the pretreatment volumetric MRI, we delineated the prostate as the automated beam-gating *target*, and a 3 mm margin around the prostate was defined as the gating window. We allowed 5% of the target to be outside the gating window for the beam to remain on (label *target in*). In contrast, if more than 5% of the target was detected outside the 3 mm gating window, the MRIdian system provided the label *target out* and a beam off was triggered. Before treatment delivery, a preview cine MRI is acquired. Subsequently, the system selects a key frame among the preview cine frames. It does so by performing deformable image registration (DIR) of a number of preview frames to the sagittal slice of the volumetric pretreatment MRI that was used for delineating the target. Automated beam-gating during treatment is based on deformations of the target between treatment cine frames and the key frame. The tracking algorithm for automated beam-gating has been described in detail by Green et al. [22]. In the event of substantial or prolonged movement of the prostate outside of the gating window, the treatment was interrupted at the discretion of the clinical staff. Such movement was typically caused by bladder or rectum filling after the acquisition of the daily MRI. In case of rapid gas passages in the rectum, the treatment could be paused and resumed without repeating the online-adaptive workflow. In case of bladder filling or stationary rectum filling, the treatment was interrupted and a partial plan, consisting of the undelivered online-adapted plan, was generated by the MRIdian system. Thus, the patient was re-scanned and the remaining dose was delivered after correcting the position of the patient in 3D. The plan was not re-optimized and the dose was not recalculated before continuing treatment. However, after treatment, partially delivered fraction doses were automatically calculated on the pre-treatment volumetric MRIs and saved in the system together with the cine MRI. General consent for data use was available for all patients and ethics approval of the study was received (BASEC-2018-01794).

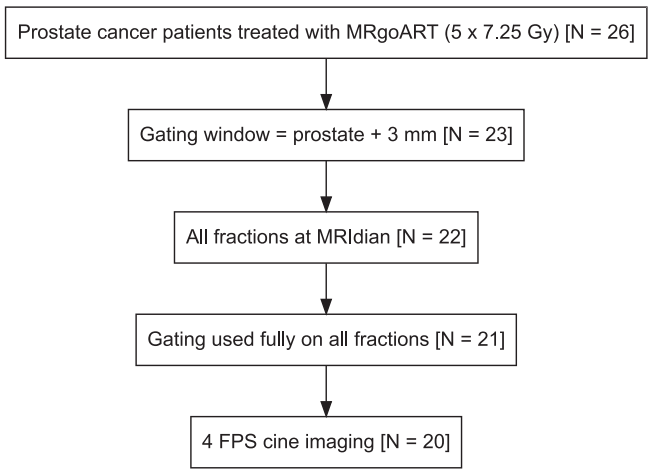

Fig. 1. Patient selection flowchart. Out of the 26 patients assessed as possible candidates for this study, 20 patients were found eligible. MRgRT = MR-guided radiotherapy and FPS = frames per second.

Motion-compensated dose calculation

We employed an in-house-developed script [23,34] written in MATLAB (The MathWorks Inc., Natick, MA) to obtain the motion-compensated dose distributions (MCDD). The MRIdian tracking algorithm automatically detects the target structure on each frame of the cine MRI and saves the target and gating window outlines onto the frame [22]. Our in-house script extracts these outlines by color thresholding, computes the convex hull, and calculates the center of mass (COM) of the target with respect to that of the gating window. Also, the gating labels (“target in” or “target out” of the gating window) are extracted for each frame. In reviewing an extensive number of treatment cine MRIs visually, we noticed that the target structure was occasionally incorrectly detected by the tracking algorithm and propagated away from the prostate and outside the gating window, e.g. into the bladder. In these frames the correlation between the visually observed position of the prostate on the cine MRIs and the position of the tracking structure was low and the system erroneously judged the prostate outside the gating window. The opposite, i.e. that the prostate would be outside of the gating window on the cine MRIs but the tracking structure would be inside the gating window, was not observed in manual review. Thus, all cine frames, where the target COM was labeled outside the gating window, were analyzed systematically. In case the tracking structure was judged erroneous, we linearly interpolated the COM of the preceding and succeeding correctly tracked frames to replace the COM of the incorrectly tracked frames. Subsequently, the script generated a 2D weight map of positions in superior-inferior (SI) and anterior-posterior (AP) directions with 1 mm resolution. Interrupted fractions were

included in the analysis by combining the motion traces from all partially delivered fractions into one. Thus, we obtained one weight map for motion during beam-on (residual motion) and another weight map including motion both during beam-on and beam-off (total motion). In order to obtain sagittal 2D MCDDs, these weight maps were used to shift and sum the daily planned static 3D dose distributions from the MRIdian system.

Dose accumulation of motion-compensated fraction doses

In order to evaluate the effect of motion in the sagittal plane on the whole treatment, we accumulated the five daily MCDDs using DIR. Daily MCDDs for residual motion and total motion, as well as the planned static dose, were accumulated. In hope of making the conclusions based on dose accumulations insensitive to the choice of DIR algorithm, we used five different DIR algorithms. Three of the algorithms depended on user input for the initial fusion of the moving and fixed image in MIM (MIM Software Inc, Cleveland, OH). The MIM algorithms included one intensity-based (from now on called MIM Intensity-based), one contour-based (MIM Contour-based), and one hybrid (MIM Hybrid) algorithm (Piper JW, Richmond JH, Nelson AS. VoxAlign Deformation Engine ® Deformable Algorithms; 2018) [24]. Furthermore, we employed the Symmetric Image Normalization method [25] in Advanced Normalization Tools (ANTs) using the default input parameters and a b-spline DIR from the Elastix [26,27] toolbox (from now on called Elastix). The parameters found for the Elastix parameter file were obtained by visual assessment of registration results. The final parameter file can be found in Supplementary file 1. The complete code for dose accumulation using ANTs and Elastix is available at GitHub [28]. All motion-compensated fraction doses were accumulated onto the pre-treatment simulation MR (MRSIM).

Dosimetric impact of beam-gating

To assess the homogeneity and conformity of the planned static dose distributions, the homogeneity index and the conformity index were calculated. The homogeneity index was defined as PTV $D_{5\%}$ divided by PTV $D_{95\%}$, and the conformity index was defined as $V_{95\%}$ (first five patients) or $V_{100\%}$ (remaining 15 patients) divided by PTV volume. Furthermore, the daily MCDDs as well as accumulated MCDDs using all five algorithms were evaluated based on $D_{95\%}$ and D_{mean} to the prostate as well as for $D_{2\%}$ to the bladder and rectum. As part of the evaluation of the dose differences we performed Wilcoxon signed-rank tests. Additionally, to evaluate the impact of prostate-to-PTV margin on prostate coverage, we simulated continuously smaller margins by increasing the prostate size in the dose matrices. We generated four structures on the MRSIM per patient by increasing the prostate isotropically by 1 mm, 2 mm, 3 mm, and 4 mm and, subsequently, subtracting the rectum structure. These structures simulate a prostate-to-PTV-margin of 4 mm, 3 mm, 2 mm, and 1 mm, respectively. The varying PTV coverage criteria ($D_{95\%} \geq 36.25$ Gy ($N = 15$) and $D_{95\%} \geq 34.44$ Gy ($N = 5$)) complicated this analysis. However, all 20 patients could be included by setting these doses equal to 100% and evaluating the prostate coverage ($D_{95\%}$) in relative dose. We evaluated the coverage of all five PTV margins for daily MCDDs and accumulated MCDDs incorporating residual motion, total motion, as well as no motion (planned static dose).

Quality assurance of the deformable image registration

We assessed the quality of the DIRs underlying the dose accumulations by computing the dice similarity coefficient (DSC) between the daily delineated prostate structure transformed to the fixed image and the prostate structure delineated on the fixed image. DSC is given as two times the volume where the contours assessed overlap, divided by their combined volume [29]. DSC was chosen since it is the most commonly reported metric in literature, intuitive, albeit a crude measure of correctness [30]. For the three DIR algorithms in MIM, we evaluated the DSC in MIM. For ANTs and Elastix we converted the prostate structure from DICOM format to a mask using an in-house-developed script [31]. Subsequently, we transformed the mask from the moving image to the fixed image using the transformations generated in ANTs and Elastix using in-house developed scripts [28]. Finally, DSC was computed using MedPy (version 0.4.0) between the mask on the fixed image and the transformed mask. In the evaluation of differences in DSCs, we performed Wilcoxon signed-rank tests.

Results

For 21 fractions of 13 patients, the dose delivery was interrupted manually. The mean ± SD (mm) COM translations with respect to the COM of the gating window was 0.0 ± 1.0 for the total AP motion, 0.4 ± 1.1 for the total SI motion, 0.0 ± 1.0 for the residual AP motion, and 0.4 ± 1.1 for the residual SI motion. The proportion of cine frames for each patient where the prostate structure was outside the gating window (labeled “target out”) ranged between 0.0% and 15.9% (Fig. 2). The median proportion of real prostate motion and tracking error was 0.3% (range 0.0% to 13.0%) and 0.9% (range 0.0% to 7.7%), respectively. Patient 12 had the highest proportion of frames with tracking errors (7.7%) and the worst prostate coverage in the initial plan. The main cause of tracking errors was poor image quality and sudden intensity changes in the cine MRIs.

The median homogeneity index of the planned static plans was 1.08 (range 1.07 to 1.09) for the first five patients, and 1.04 (range 1.04 to 1.06) for the remaining 15 patients. The median conformity index was 1.23 (range 1.07 to 1.25) for the first five patients, and 1.15 (range 1.09 to 1.29) for the remaining 15 patients.

We are only presenting dose accumulation results obtained with the MIM Hybrid algorithm in the main text. This algorithm agrees with the rest of the algorithms regarding the dosimetric impact of gating on prostate coverage (Fig. 3A and Fig. S1 in Supplementary file 1) and gives median results in the PTV margin simulation (Fig. 4 and Fig. S4 in Supplementary file 1). Differences between accumulated MCDDs of residual and total motion were of negligible magnitude for all dose metrics assessed (Table 1 and blue symbols in Fig. 3). The same was true for accumulated MCDDs of residual motion compared to planned static dose (Table 1 and orange symbols in Fig. 3). The largest difference in $D_{95\%}$ and D_{mean} between residual accumulated MCDDs and planned static doses was observed for patient 12 (0.4 Gy and 0.2 Gy, respectively). Dose accumulations with the four other DIR algorithms agreed with the results for MIM Hybrid that there is a negligible dosimetric impact on prostate $D_{95\%}$ coverage (Fig. S1 in Supplementary file 1). There was a small median decrease in bladder and rectum $D_{2\%}$ for gated treatments compared to planned static dose (Table 1 and orange symbols in Fig. 3C and D). Regarding daily MCDDs, differences between residual MCDDs on the one hand and total motion MCDDs or planned static dose on the other hand were negligible (Table 1 and Fig. S2 and Fig. S3 in Supplementary file 1).

Accounting only for motion, prostate-to-PTV margin simulations showed that 18 of 20 patients would have received a prostate $D_{95\%}$ coverage above 100% of the prescription dose with a margin of 3 mm, instead of the clinically used margin of 5 mm, even without gating (Fig. 4). This was true for 20, 19, 18, and 17 patients according to MIM Contour-based, MIM Intensity-based, ANTs, and Elastix,

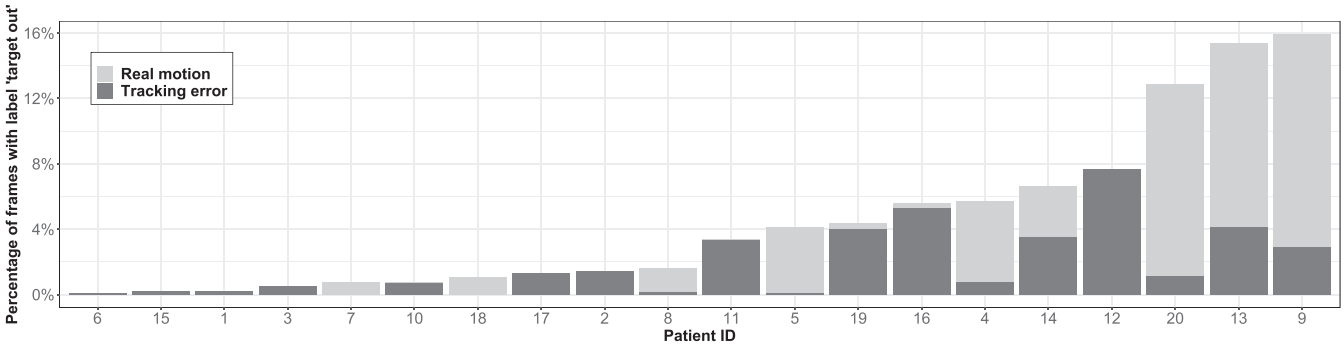

Fig. 2. Proportion of frames with target labelled "target out". Dark grey indicates frames where the prostate was visually assessed to be within the tracking gating window (i.e. tracking error). Light grey indicates frames visually assessed as real prostate motion.

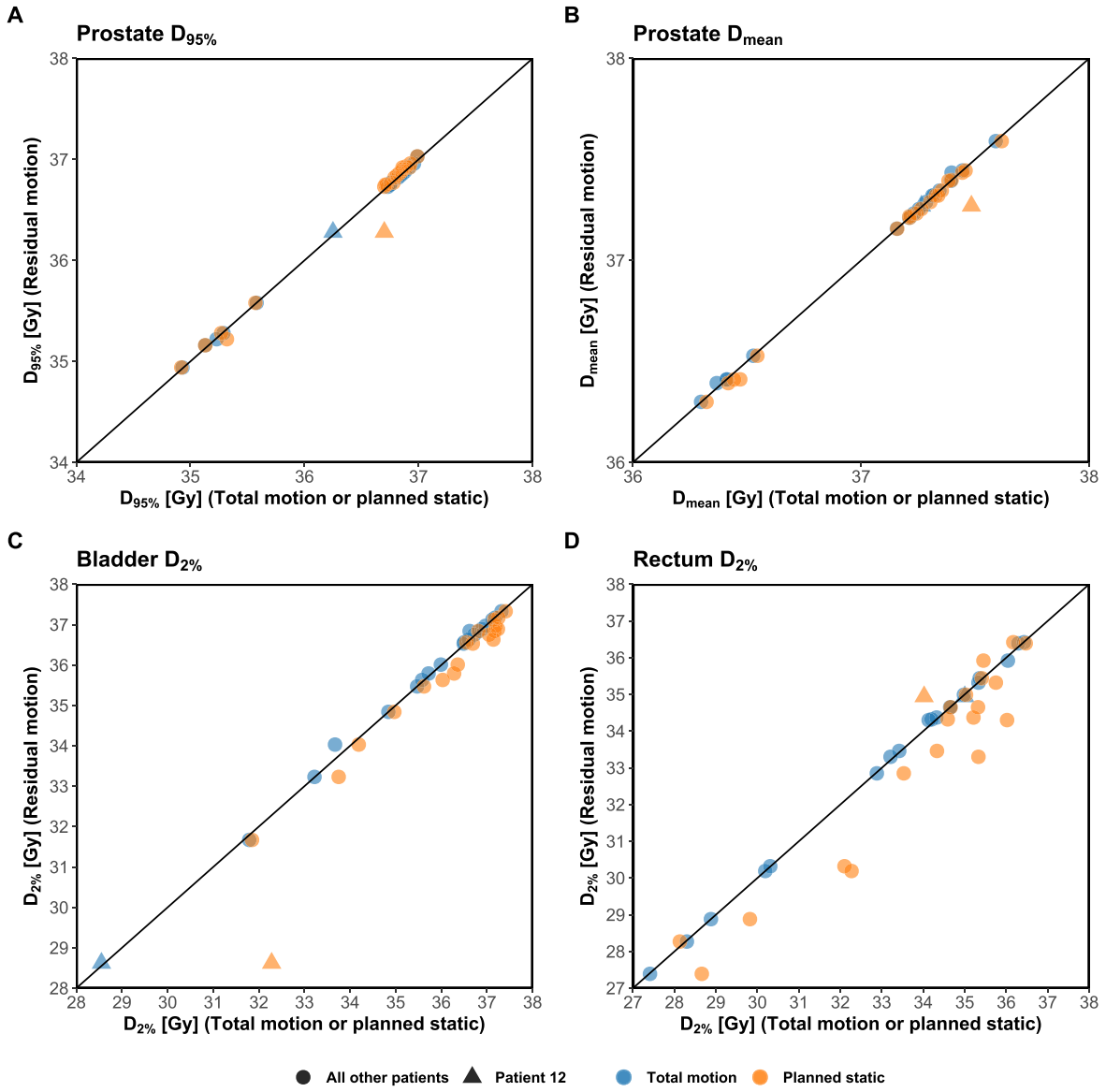

Fig. 3. Dosimetric evaluation of the impact of beam-gating. Motion-compensated dose accumulations incorporating residual prostate motion versus motion-compensated dose accumulations incorporating total prostate motion (blue) and versus the accumulated planned static dose (orange) for (A) prostate $D_{95\%}$, (B) prostate mean dose, (C) bladder $D_{2\%}$, and (D) rectum $D_{2\%}$. The dose accumulations were performed with the MIM hybrid algorithm.

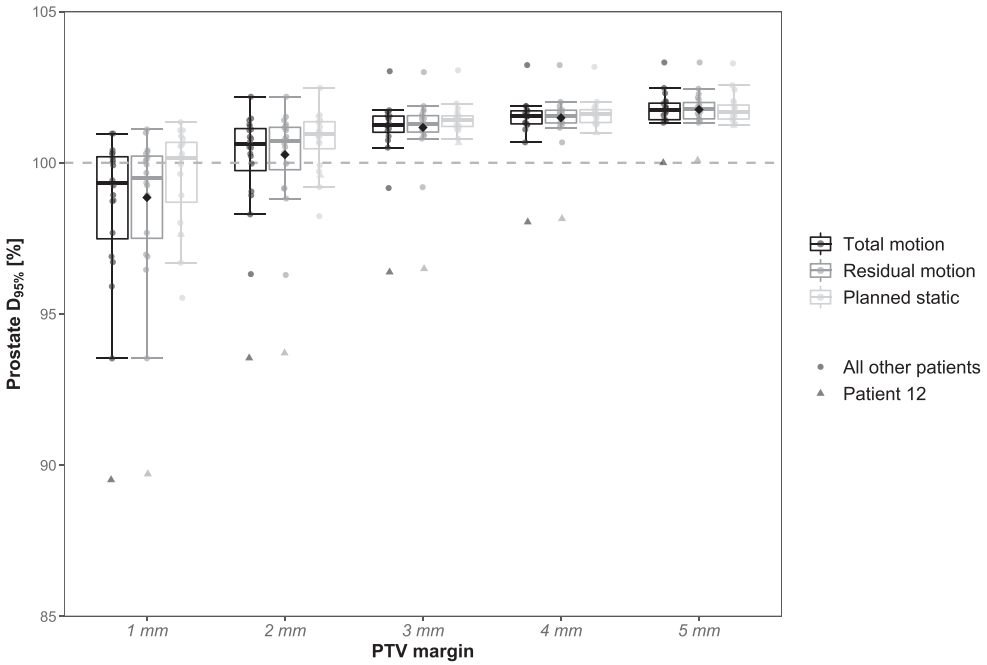

Fig. 4. Simulations of the impact of PTV margin on target coverage (prostate $D_{95\%}$). Motion-compensated dose accumulations incorporating residual prostate motion (black) and motion-compensated dose accumulations incorporating total prostate motion (grey) as well as planned static (light grey). The accumulations were performed with the MIM hybrid algorithm.

Table 1
Dosimetric analysis of impact of beam-gating and impact of motion compared to planned static dose. Daily motion-compensated dose distributions (MCDDs) are scaled to total treatment dose.

			Median [Range] difference (I-J) in Gy			
	(I)	(J)	Prostate $D_{95\%}$	Prostate D_{mean}	Bladder $D_{2\%}$	Rectum $D_{2\%}$
Accumulated MCDDs	Residual	Total	0.00 [−0.01 to 0.04]*	0.00 [0.00 to 0.04]***	0.02 [−0.12 to 0.36]*	0.00 [−0.12 to 0.17]
		Planned static	0.03 [−0.42 to 0.06]*	−0.01 [−0.21 to 0.01]***	−0.20 [−3.66 to 0.03]***	−0.55 [−2.08 to 0.92]**
Daily MCDDs	Residual	Total	0.00 [−0.03 to 0.10]	0.00 [−0.03 to 0.11]***	0.00 [−0.27 to 0.80]***	0.00 [−0.67 to 1.09]
		Planned static	0.14 [−0.15 to 0.27]***	0.00 [−0.15 to 0.19]***	−0.21 [−1.89 to 1.05]***	−0.72 [−5.44 to 2.34]***

p-value. *: $p < 0.05$, **: $p < 0.01$, ***:$p < 0.001$.

respectively (Fig. S4\1 in Supplementary file 1) and for 99 of 100 delivered fractions (Fig. S5 in Supplementary file 1). With a 3 mm margin, fraction 2 for patient 12 was the only fraction with a prostate $D_{95\%}$ lower than 100% (Fig. S5 in Supplementary file 1). This fraction had the largest proportion of tracking errors and the cine MRIs are dominated by radiofrequency spike artifacts, poor image contrast, and sudden changes in gray value intensities, making the tracking of the prostate inaccurate.

For the patient with the highest proportion of frames with real motion during treatment (patient 9), a 1 mm prostate-to-PTV margin would still have sufficed to ensure a prostate $D_{95\%}$ above 100% incorporating residual motion (Fig. 5A). For patient 12, a 4 mm margin would have been required to ensure the same prostate coverage (Fig. 5B). The conformity and homogeneity indexes were 1.29 and 1.04, respectively, for patient 9 and 1.09 and 1.06, respectively, for patient 12.

The mean DSC per patient, expressed as median (range), for ANTs, Elastix, MIM Contour-based, MIM Hybrid, and MIM Intensity-based were 0.91 (0.84 to 0.94), 0.89 (0.82 to 0.94), 0.95 (0.93 to 0.96), 0.90 (0.87 to 0.94), , and 0.91 (0.87 to 0.94), respectively (Fig. S6).The highest DSC was found for MIM Contour-based, which is to be expected as this algorithm minimizes the signed distances between the evaluated contours.

Discussion

Due to superior soft tissue contrast, real-time monitoring, and automated real-time beam-gating, MR-linac systems could potentially improve accuracy in dose delivery [13,32]. This would, in turn, enable PTV margin reductions with the benefits of lowering dose to OARs or allowing higher doses to the tumor [13,32]. Nevertheless, this study is the first to evaluate the potential dosimetric impact of beam-gating in MRgRT of prostate cancer. This study suggests that treating prostate cancer with online-adaptive MRgRT in five fractions or more on a MRIdian machine prescribed with a PTV coverage of $D_{95\%} \geq 100\%$ of the prescription dose and with a clinical prostate-to-PTV margin of 3 mm posteriorly and 5 mm in the remaining directions is safe, both with and without gating. Furthermore, our study indicates that the clinically used PTV margin could potentially be reduced to a 3 mm expansion of the prostate and still secure $D_{95\%} \geq 100\%$. According to our PTV margin simulation (Fig. 4 as well as Fig. S4, and Fig. S5 in Supplementary file 1), there is little coverage difference between applying the gating window settings used in this study (3 mm, 5%) and not gating at all for all PTV margins assessed. Thus, relaxing the clinically employed gating window settings for the patients in this study would not have affected the conclusion regarding PTV margin or the impact

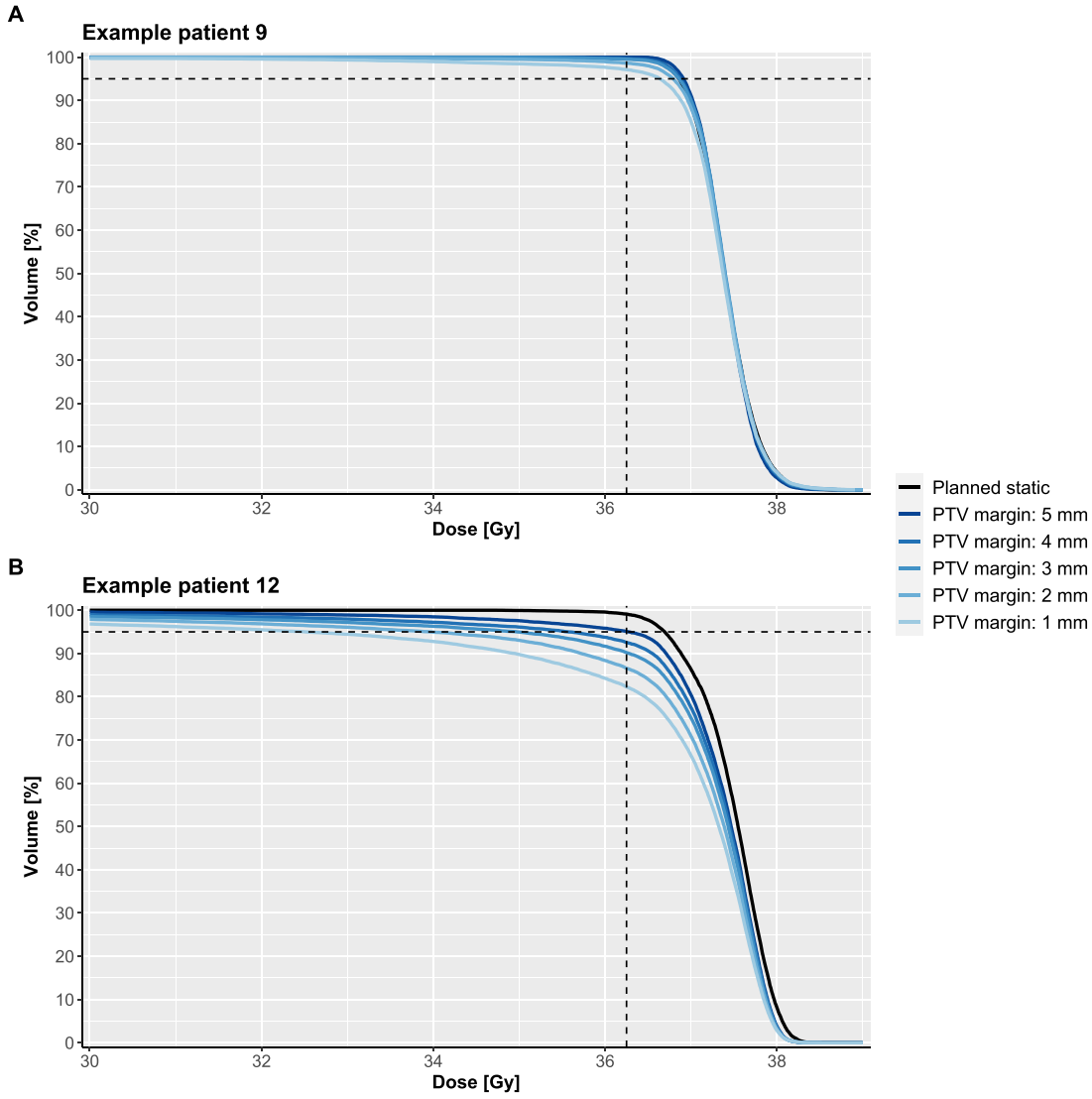

Fig. 5. Prostate DVHs incorporating residual motion for different PTV margins for two example patients. A) The patient with the largest proportion of frames with real motion (patient 9), and B) the patient with the poorest planned prostate coverage (patient 12). The intersection of the dashed lines indicates the clinical prescription dose to the prostate ($D_{95\%} \geq 36.25$ Gy). The accumulations were performed with the MIM Hybrid algorithm.

of gating as long as there is visual inspection by treatment staff. The effect of tightening the gating windows settings (below 3 mm, 5%) on prostate coverage and on necessary PTV margins remains an open question.

In this study, a negligible dosimetric impact of beam-gating (residual intrafraction motion versus total motion) on prostate $D_{95\%}$[Gy] of 0.00 (-0.03 to 0.10), expressed as median (range) of 100 treatment fractions, was found. This appears to be in contradiction with De Roover et al. [15]. They reported that gating improved CTV $D_{95\%}$[%] with median (range) 0.8 (−2.7 to 5.1). However, two of the three traces employed by De Roover et al. [15] contained 2D shifts above 2 mm for 60% and 80% of the treatment time, respectively, and one of the traces contained 2D shifts above 6 mm for more than 40% of the time. Thus, these experimentally employed traces contain more movement than the mean ± SD (mm) COM translations of 0.0 ± 1.0 (AP) and 0.4 ± 1.1 (SI) observed for the 100 real treatment fractions analyzed in this study. Colvill et al. [18] found that motion in one fraction reduced coverage (CTV $D_{99\%}$) with more than 19% without gating compared to below 4% when gating was applied. However, the 20 motion traces employed by Colvill et al. [18] were all hand-picked either because they contained a certain type of intrafractional prostate motion ($N = 6$) or because they displayed high mean prostate displacement ($N = 13$). Thus, Colvill et al. [18], concludes that gating is unlikely to influence the overall treatments for most conventionally fractionated prostate treatments. Our results show that the same can be concluded for online-adapted MR-guided prostate SBRT with online monitoring.

We found negligible coverage increases in terms of prostate $D_{95\%}$ for MCDDs compared to planned static dose, with a median absolute increase of 0.14 Gy and 0.03 Gy for daily and accumulated MCDDs, respectively. These numbers apply both to residual and total MCDDs compared to planned static dose. This increase in coverage when motion is incorporated could possibly be due to prostate motion in the anterior direction, away from the rectum, where the PTV margin was the smallest. Other studies have found coverage decreases for MCDDs compared to planned static dose. Kontaxis et al. [19] and Menten et al. [20] both reconstructed dose for five prostate cancer patients treated on an Elekta Unity MR-linac. They found average CTV coverage decreases between MCDDs

and planned static dose of 2.2% ($D_{99\%}$) and 1.1 Gy ($D_{98\%}$), respectively. Our study found small decreases in near-maximum ($D_{2\%}$) doses to the bladder and rectum both for daily and accumulated MCDDs compared to planned static dose. Both Kontaxis et al. [19] and Menten et al. [20] agreed that the near-maximum dose to the rectum decreases comparing MCDDs to planned static dose. This decrease is probably due to the blurring of the high dose areas accomplished by motion. Menten et al. [20] agreed with our study in finding small differences in near-maximum doses to the bladder when motion was accounted for. However, Kontaxis et al. [19] reported an increase in average near-maximum dose to the bladder of 1.6%. As opposed to both studies, our study did not incorporate timestamped data of linac parameters in the dose reconstruction, as this is not available in the MRIdian system. On the other hand, our study utilized interfractional dose accumulation, which was not attempted in either of the aforementioned studies.

A limitation of this study is that the automatic tracking of the prostate by the MRIdian system occasionally failed to provide reliable positions of the prostate during treatment. The main reasons for tracking failure were spike artifacts, poor image contrast, and sudden changes in gray value intensities. We tried to reduce the impact of poor tracking by manually replacing cine frames for which we visually assessed that the prostate position was wrongly labeled as outside the gating window. Another limitation is that our study did not take prostate motion in the left–right direction into account. However, several studies have found that motion in the SI and AP directions are significantly larger than in the left–right direction [33] and thus we assume that the largest prostate motions for these patients were considered. Regarding safety margins, there are more uncertainties than intrafractional motion that will influence them. However, according to the ESTRO ACROP consensus guideline on the use of image guided radiation therapy for localized prostate cancer [10], only intrinsic uncertainties of the image-guided radiotherapy system (0.5–1.5 mm, 1SD) and intrafraction residual errors remain when real-time prostate tracking is used. As a result, they recommend a range of prostate-to-PTV margins between 2 and 4 mm as plausible for prostate-only EBRT in five fractions using real-time prostate tracking. This is in agreement with the 3 mm prostate-to-PTV margin found in this study. However, the impact of motion on prostate coverage, and thus also on the necessary safety margins, is dependent on the conformity of the planned static dose. This partly explains why the prostate coverage for patient 9 (planned static dose conformity index 1.29) is more robust against motion than the prostate coverage for patient 12 (planned static dose conformity index 1.09), see Fig. 5. One should bear in mind that our prostate-to-PTV margin simulation, accomplished by increasing the prostate structure in the motion-compensated dose distributions, is presumably more conservative than a full replanning on multiple PTV margins. First, treatment planning to a smaller PTV implies less compromises with the rectum, implying better prostate coverage in the posterior direction. Second, treatment planning based on a small PTV implies less beam divergence and thus higher conformality than treatment planning on a larger PTV. Thus, it appears safe to reduce margins for these patients, in order to achieve benefits in terms of lower dose to nearby healthy tissue.

Conclusion

Beam-gating has negligible dosimetric impact in online-adaptive MRgRT of prostate cancer over five or more fractions. Delivering online-adaptive MRgRT SBRT of prostate cancer on the MR-linac was assessed safe with the PTV margins used clinically. For 18 out of 20 patients, the clinically used prostate-to-PTV margin of 5 mm could potentially have been reduced to 3 mm while still retaining 95% coverage of the prescription dose even without the beam-gating.

Conflict of interest statement

Isak Wahlstedt's Ph.D. studies are partly funded by Danish Comprehensive Cancer Center and ViewRay. Nicolaus Andratschke reports research grants, speaker honorary, and travel grants from Brainlab and ViewRay. Claus P. Behrens reports research contracts with Brainlab, Varian, and ViewRay outside of the submitted work. Ivan R Vogelius reports institutional research and teaching contracts with Brainlab, Varian, and ViewRay. Stefanie Ehrbar, Hubert S. Gabryś, Helena Garcia Schüler, Matthias Guckenberger, Abraham George Smith, Stephanie Tanadini-Lang, José D. Tascón-Vidarte, and Janita E. van Timmeren report no conflict of interest.

Acknowledgements

Isak Wahlstedt's Ph.D. studies are partly funded by Danish Comprehensive Cancer Center and ViewRay. Rasmus Hvass Hansen is acknowledged for his help in identifying the artifacts seen in the cine MRIs for patient 12, fraction 2.

Appendix A. Supplementary data

Supplementary data to this article can be found online at https://doi.org/10.1016/j.radonc.2022.03.013.

References

[1] Kalbasi A, Li J, Berman AT, Swisher-McClure S, Smaldone M, Uzzo RG, et al. Dose-escalated irradiation and overall survival in men with nonmetastatic prostate cancer. JAMA Oncol 2015;1:897.
[2] Catton CN, Lukka H, Gu C-S, Martin JM, Supiot S, Chung PWM, et al. Randomized trial of a hypofractionated radiation regimen for the treatment of localized prostate cancer. J Clin Oncol 2017;35:1884–90.
[3] Dearnaley D, Syndikus I, Mossop H, Khoo V, Birtle A, Bloomfield D, et al. Conventional versus hypofractionated high-dose intensity-modulated radiotherapy for prostate cancer: 5-year outcomes of the randomised, non-inferiority, phase 3 CHHiP trial. Lancet Oncol 2016;17:1047–60.
[4] Incrocci L, Wortel RC, Alemayehu WG, Aluwini S, Schimmel E, Krol S, et al. Hypofractionated versus conventionally fractionated radiotherapy for patients with localised prostate cancer (HYPRO): final efficacy results from a randomised, multicentre, open-label, phase 3 trial. Lancet Oncol 2016;17:1061–9.
[5] Lee WR, Dignam JJ, Amin MB, Bruner DW, Low D, Swanson GP, et al. Randomized phase III noninferiority study comparing two radiotherapy fractionation schedules in patients with low-risk prostate cancer. J Clin Oncol 2016;34:2325–32.
[6] Widmark A, Gunnlaugsson A, Beckman L, Thellenberg-Karlsson C, Hoyer M, Lagerlund M, et al. Ultra-hypofractionated versus conventionally fractionated radiotherapy for prostate cancer: 5-year outcomes of the HYPO-RT-PC randomised, non-inferiority, phase 3 trial. The Lancet 2019;394:385–95.
[7] Kerkmeijer LGW, Groen VH, Pos FJ, Haustermans K, Monninkhof EM, Smeenk RJ, et al. Focal boost to the intraprostatic tumor in external beam radiotherapy for patients with localized prostate cancer: results from the FLAME randomized phase III trial. J Clin Oncol 2021;39:787–96.
[8] Draulans C, van der Heide UA, Haustermans K, Pos FJ, van der Voort van Zyp J, De Boer H, et al. Primary endpoint analysis of the multicentre phase II hypo-FLAME trial for intermediate and high risk prostate cancer. Radiother Oncol 2020;147:92–8.
[9] Greco C, Pares O, Pimentel N, Louro V, Santiago I, Vieira S, et al. Safety and efficacy of virtual prostatectomy with single-dose radiotherapy in patients with intermediate-risk prostate cancer: results from the PROSINT phase 2 randomized clinical trial. JAMA Oncol 2021;7:700.
[10] Ghadjar P, Fiorino C, Munck af Rosenschöld P, Pinkawa M, Zilli T, van der Heide UA. ESTRO ACROP consensus guideline on the use of image guided radiation therapy for localized prostate cancer. Radiother Oncol 2019;141:5–13.
[11] Schweikard A, Shiomi H, Adler J. Respiration tracking in radiosurgery. Med Phys 2004;31:2738–41. https://doi.org/10.1118/1.1774132.
[12] Poulsen PR, Cho B, Langen K, Kupelian P, Keall PJ. Three-dimensional prostate position estimation with a single x-ray imager utilizing the spatial probability density. Phys Med Biol 2008;53:4331–53. https://doi.org/10.1088/0031-9155/53/16/008.
[13] Hunt A, Hansen VN, Oelfke U, Nill S, Hafeez S. Adaptive Radiotherapy Enabled by MRI Guidance. Clin Oncol 2018;30:711–9. https://doi.org/10.1016/j.clon.2018.08.001.

[14] Klüter S. Technical design and concept of a 0.35 T MR-Linac. Clin Transl Radiat Oncol 2019;18:98–101. https://doi.org/10.1016/j.ctro.2019.04.007.
[15] De Roover R, Hansen R, Crijns W, Muurholm CG, Poels K, Skouboe S, et al. Dosimetric impact of intrafraction prostate rotation and accuracy of gating, multi-leaf collimator tracking and couch tracking to manage rotation: An end-to-end validation using volumetric film measurements. Radiother Oncol 2021;156:10–8.
[16] Ehrbar S, Schmid S, Jöhl A, Klöck S, Guckenberger M, Riesterer O, et al. Validation of dynamic treatment-couch tracking for prostate SBRT. Med Phys 2017;44:2466–77.
[17] Ehrbar S, Schmid S, Jöhl A, Klöck S, Guckenberger M, Riesterer O, et al. Comparison of multi-leaf collimator tracking and treatment-couch tracking during stereotactic body radiation therapy of prostate cancer. Radiother Oncol 2017;125:445–52.
[18] Colvill E, Poulsen PR, Booth JT, O'Brien RT, Ng JA, Keall PJ. DMLC tracking and gating can improve dose coverage for prostate VMAT: DMLC tracking and gating dose for prostate VMAT. Med Phys 2014;41. https://doi.org/10.1118/1.4892605.
[19] Kontaxis C, de Muinck Keizer DM, Kerkmeijer LGW, Willigenburg T, den Hartogh MD, van der Voort van Zyp JRN, et al. Delivered dose quantification in prostate radiotherapy using online 3D cine imaging and treatment log files on a combined 1.5T magnetic resonance imaging and linear accelerator system. Phys Imaging. Radiat Oncol 2020;15:23–9.
[20] Menten MJ, Mohajer JK, Nilawar R, Bertholet J, Dunlop A, Pathmanathan AU, et al. Automatic reconstruction of the delivered dose of the day using MR-linac treatment log files and online MR imaging. Radiother Oncol 2020;145:88–94.
[21] Cuccia F, Corradini S, Mazzola R, Spiazzi L, Rigo M, Bonù ML, et al. MR-guided hypofractionated radiotherapy: current emerging data and promising perspectives for localized prostate cancer. Cancers 2021;13:1791.
[22] Green OL, Rankine LJ, Cai B, Curcuru A, Kashani R, Rodriguez V, et al. First clinical implementation of real-time, real anatomy tracking and radiation beam control. Med Phys 2018;45:3728–40.
[23] Ehrbar S. MR-guided beam gating: Residual motion, gating efficiency and dose reconstruction for stereotactic treatments of the liver and lung. Unpublished results.
[24] SU-FF-I-68: Evaluation of An Intensity-Based Free-Form Deformable Registration Algorithm - Piper - 2007 - Medical Physics - Wiley Online Library n.d. https://aapm.onlinelibrary.wiley.com/doi/abs/10.1118/1.2760445 (accessed December 9, 2021).
[25] Avants B, Epstein C, Grossman M, Gee J. Symmetric diffeomorphic image registration with cross-correlation: evaluating automated labeling of elderly and neurodegenerative brain. Med Image Anal 2008;12:26–41. https://doi.org/10.1016/j.media.2007.06.004.
[26] Klein S, Staring M, Murphy K, Viergever MA, Pluim J. elastix: A toolbox for intensity-based medical image registration. IEEE Trans Med Imaging 2010;29:196–205. https://doi.org/10.1109/TMI.2009.2035616.
[27] Shamonin D. Fast parallel image registration on CPU and GPU for diagnostic classification of Alzheimer's disease. Front Neuroinformatics 2013;7. https://doi.org/10.3389/fninf.2013.00050.
[28] Tascón-Vidarte JD. GitHub – josetascon/dose-accumulation: Interfraction dose accumulation for radiotherapy using deformable image registration n.d. https://github.com/josetascon/dose-accumulation (accessed November 25, 2021).
[29] Brock KK, Mutic S, McNutt TR, Li H, Kessler ML. Use of image registration and fusion algorithms and techniques in radiotherapy: Report of the AAPM Radiation Therapy Committee Task Group No. 132. Med Phys 2017;44:e43–76.
[30] Sharp G, Fritscher KD, Pekar V, Peroni M, Shusharina N, Veeraraghavan H, et al. Vision 20/20: Perspectives on automated image segmentation for radiotherapy: Perspectives on automated image segmentation for radiotherapy. Med Phys 2014;41:050902. https://doi.org/10.1118/1.4871620.
[31] Smith AG. Abe404/dicom_mask: 0.0.17b | Zenodo n.d. https://zenodo.org/record/5727328#.YaUnoWDMKUl (accessed November 29, 2021).
[32] McPartlin AJ, Li XA, Kershaw LE, Heide U, Kerkmeijer L, Lawton C, et al. MRI-guided prostate adaptive radiotherapy – A systematic review. Radiother Oncol 2016;119:371–80.
[33] Byrne TE. A review of prostate motion with considerations for the treatment of prostate cancer. Med Dosim 2005;30:155–61. https://doi.org/10.1016/j.meddos.2005.03.005.
[34] https://www.estro.org/Congresses/ESTRO-2021/509/profferedpapers21-motionmanagement/3728/whattoexpectfrommr-guidedbeamgating-residualmotion. [Accessed 1 April 2022].